

Enhanced symmetry energy bears universality of the r-process

José Nicolás Orce^{a,b,*}, Balaram Dey^c, Cebo Ngwetsheni^a, Srijit Bhattacharya^d, Deepak Pandit^{e,f}, Brenden Lesch^a, Andile Zulu^a

^aDepartment of Physics & Astronomy, University of the Western Cape, P/B X17, Bellville ZA-7535, South Africa

^bNational Institute for Theoretical and Computational Sciences (NITheCS), South Africa

^cDepartment of Physics, Bankura University, Bankura-722155, West Bengal, India

^dDepartment of Physics, Barasat Govt. College, Barasat, West Bengal-700124, India

^eVariable Energy Cyclotron Centre, 1/AF-Bidhannagar, Kolkata-700064, India

^fHomi Bhabha National Institute, Training School Complex, Anushaktinagar, Mumbai 400094, India

Abstract

The abundance of about half of the stable nuclei heavier than iron via the rapid neutron capture process or r-process is intimately related to the competition between neutron capture and β -decay rates, which ultimately depends on the binding energy of neutron-rich nuclei. The well-known Bethe-Weizsäcker semi-empirical mass formula[1, 2] describes the binding energy of ground states – i.e. nuclei with temperatures of $T \approx 0$ MeV – with the symmetry energy parameter converging between 23–27 MeV for heavy nuclei. Here we find an unexpected enhancement of the symmetry energy at higher temperatures, $T \approx 0.7$ –1.0 MeV, from the available data of giant dipole resonances built on excited states. Although these are likely the temperatures where seed elements are created – during the cooling down of the ejecta following neutron-star mergers[3] or collapsars[4] – the fact that the symmetry energy remains constant between $T \approx 0.7$ –1.0 MeV, suggests a similar trend down to $T \approx 0.5$ MeV, where neutron-capture may start occurring. Calculations using this relatively larger symmetry energy yield a reduction of the binding energy per nucleon for heavy neutron-rich nuclei and inhibits radiative neutron-capture rates. This results in a substantial close in of the neutron dripline – where nuclei become unbound – which elucidates the long sought universality of heavy-element abundances through the r-process; as inferred from the similar abundances found in extremely metal-poor stars and the Sun.

Keywords: symmetry energy, dipole polarizability, photo-absorption cross sections, r-process, neutron dripline

The binding energy of a nucleus with Z protons and N neutrons can be described by the well-known Bethe-Weizsäcker semi-empirical mass formula (SEMF) [1, 2],

$$B(Z, A) = a_v A - a_s A^{2/3} - a_c Z(Z-1)A^{-1/3} - a_{\text{sym}} \frac{(A-2Z)^2}{A} \pm a_p A^{-3/4}, \quad (1)$$

where $A = Z + N$ is the mass number and a_v , a_s , a_c , a_{sym} and a_p are the volume, surface, Coulomb, symmetry energy and pairing coefficients, respectively. The symmetry energy, $a_{\text{sym}}(A)(N-Z)^2/A$, reduces the total binding energy $B(Z, A)$ of a nucleus as the neutron-proton asymmetry becomes larger, i.e. for $N \gg Z$, and yields the

typical negative slope of the binding energy curve[5] for $A > 62$. It is divided by A to reduce its importance for heavy nuclei, and it depends on the mass dependency of $a_{\text{sym}}(A)$. Its convergence for heavy nuclei establishes the frontiers of the neutron dripline for particle-unbound nuclei and eventually leads to the disappearance of protons at extreme nuclear densities[6].

Furthermore, $a_{\text{sym}}(A)$ is relevant to understanding neutron skins[7], the effect of three-nucleon forces[8] and – through the equation of state (EoS) – supernovae cores, neutron stars and binary mergers[9–11]. The latter are the first known astrophysical site where heavy elements are created through the rapid neutron-capture or r-process[12, 13]. The identification of heavy elements in neutron star mergers is supported by the short duration gamma-ray bursts via their infrared afterglow[14] – only understood by the opacities of heavy nuclei – as well as blueshifted Sr II absorption lines[15], following

*Corresponding author

Email address: jnorce@uwc.ac.za (José Nicolás Orce)

URL: <https://nuclear.uwc.ac.za> (José Nicolás Orce)

the expansion speed of the ejecta gas at $v = 0.1 - 0.3 c$. Mergers are expected to be the only source for the creation of elements above lead and bismuth, as inferred from the very scarce abundance of actinides in the solar system[16].

The universality of the r-process for the heaviest elements with $56 < Z < 90$ is further inferred from the similar abundance patterns observed in both extremely metal-poor stars and the Sun[17, 18]. Other potential sources of heavy elements involve different types of supernova (e.g. collapsars [4] – the supernova-triggering collapse of rapidly rotating massive stars – and type-II supernova[12]), which need to be considered in order to explain all neutron-capture abundances[19, 20].

It is the motivation of this work to understanding the limits of the neutron dripline and heavy-element production by investigating $a_{\text{sym}}(A)$ at different temperatures T using available data of potential interest to the r-process; namely, data from photoabsorption cross sections, binding energies and giant dipole resonances.

Generally, $a_{\text{sym}}(A)$ is parametrized using the leptodermous approximation of Myers and Swiatecki, where $A^{-1/3} \ll 1$ [21],

$$a_{\text{sym}}(A) = S_v \left(1 - \frac{S_s}{S_v} A^{-1/3} \right), \quad (2)$$

which considers the modification of the volume symmetry energy, S_v , by the surface symmetry energy S_s . This particular leptodermous parametrization was chosen on the account of its better fit to the masses of isobaric nuclei [22]. Constraints on these parameters have been investigated using experimental and theoretical information concerning properties of ground states, i.e. at $T = 0$ MeV[23, 24].

The giant dipole resonance (GDR) represents the main contribution to the absorption and emission of electromagnetic radiation (photons) in nuclei[25]. The dynamics of this quantum collective excitation is characterized by the inter-penetrating motion of proton and neutron fluids out of phase[26], which results from the density-dependent symmetry energy, $a_{\text{sym}}(A)(\rho_N - \rho_Z)^2/\rho$, acting as a restoring force[25]; where ρ_N , ρ_Z and $\rho = \rho_N + \rho_Z$ are the neutron, proton and total density, respectively, which spread uniformly throughout the nucleus.

The ratio of the induced dipole moment to an applied constant electric field yields the static nuclear polarizability, α . Using the hydrodynamic model and assuming inter-penetrating proton and neutron fluids with a well-defined nuclear surface of radius $R = r_0 A^{1/3}$ fm and ρ_Z as the potential energy of the liquid drop, Migdal[26]

obtains the following relation between the static nuclear polarizability, α , and a_{sym} ,

$$\alpha = \frac{e^2 R^2 A}{40 a_{\text{sym}}} = 2.25 \times 10^{-3} A^{5/3} \text{ fm}^3, \quad (3)$$

where $r_0 = 1.2$ fm, $e^2 = 1.44$ MeV fm in the c.g.s. system, and a constant value of $a_{\text{sym}} = 23$ MeV was utilized.

Alternatively, α can be calculated for the ground states of nuclei using second-order perturbation theory[27] following the sum rule,

$$\alpha = 2e^2 \sum_n \frac{\langle i || \hat{E}1 || n \rangle \langle n || \hat{E}1 || i \rangle}{E_\gamma} \quad (4)$$

$$= \frac{e^2 \hbar^2}{M} \sum_n \frac{f_{in}}{E_\gamma^2} = \frac{\hbar c}{2\pi^2} \int_0^\infty \frac{\sigma_{\text{total}}(E_\gamma)}{E_\gamma^2} dE_\gamma \quad (5)$$

$$= \frac{\hbar c}{2\pi^2} \sigma_{-2}, \quad (6)$$

where E_γ is the γ -ray energy corresponding to a transition connecting the ground state $|i\rangle$ and an excited state $|n\rangle$, M the nucleon mass, f_{in} the dimensionless oscillator strength for E1 transitions [27] and σ_{-2} the second moment of the total electric-dipole photo-absorption cross section,

$$\sigma_{-2} = \int_0^\infty \frac{\sigma_{\text{total}}(E_\gamma)}{E_\gamma^2} dE_\gamma, \quad (7)$$

where $\sigma_{\text{total}}(E_\gamma)$ is the total photo-absorption cross section, which generally includes $(\gamma, n) + (\gamma, pn) + (\gamma, 2n) + (\gamma, 3n)$ photoneutron and available photoproton and photofission cross sections [28], in competition in the GDR region [29, 30]. By comparing Eqs. 3 and 6, a mass-dependent symmetry energy, $a_{\text{sym}}(A)$, is extracted in units of MeV,

$$a_{\text{sym}}(A) = \frac{e^2 R^2 \pi^2 A}{20 \hbar c \sigma_{-2}} \approx 5.2 \times 10^{-3} \frac{A^{5/3}}{\sigma_{-2}}. \quad (8)$$

Empirical evaluations reveal that σ_{-2} can also be approximated by $\sigma_{-2} = 2.4 \kappa A^{5/3}$, where the dipole polarizability parameter κ measures GDR deviations between experimental and hydrodynamic model predictions[31].

Figure 1 shows the distribution of $a_{\text{sym}}(A)$ for the ground state of stable isotopes, along the nuclear landscape, determined from empirical σ_{-2} values. Data include all available emission channels. The contribution of (γ, p) cross sections are evident in light nuclei, which significantly reduces the symmetry energy. For heavy nuclei, (γ, n) cross sections are dominant because of the higher Coulomb barrier. A fit

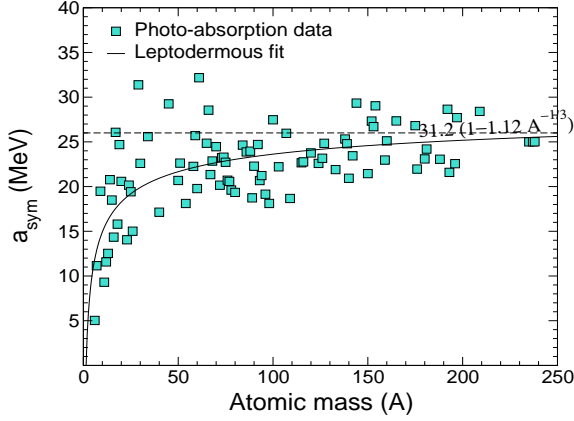


Figure 1: Symmetry energy coefficient, $a_{\text{sym}}(A)$, of finite nuclei as a function of mass number A extracted from the experimental σ_{-2} values extracted from available photoabsorption cross-sections[32, 33], as given in Eq. 8 and fitted (solid line) by Eq. 2.

to the data using Eq. 2 (solid line) yields $a_{\text{sym}}(A) = 31.2(12) (1 - 1.12(10)A^{-1/3})$ MeV, with an RMS deviation of 22%[34]. Unfortunately, (γ, p) cross-section data are very scarce, which directly affects the $a_{\text{sym}}(A)$ trend for $A \lesssim 70$ in Fig. 1.

In addition, Tian and co-workers determined $a_{\text{sym}}(A) = 28.32 (1 - 1.27A^{-1/3})$ MeV from a global fit to the binding energies of isobaric nuclei with mass number $A \geq 10$ [22] – extracted from the 2012 atomic mass evaluation[35] – with $S_v \approx 28.32$ MeV being the bulk symmetry energy coefficient and $\frac{S_s}{S_v} \approx 1.27$ the surface-to-volume ratio. Similar coefficients are calculated in Refs.[9, 36]. Within this approach, the extraction of $a_{\text{sym}}(A)$ only depends on the Coulomb energy term in the SEMF and shell effects[37] – which are both included [22] – and $a_{\text{sym}}(A)$ presents a maximum energy around 23 MeV. This description of $a_{\text{sym}}(A)$ has been used to explain the enhanced σ_{-2} values observed for low-mass nuclei[34].

The symmetry energy $a_{\text{sym}}(A)$ is the fundamental parameter that characterizes the energy of the GDR, E_{GDR} , within the Steinwedel-Jensen (SJ) model of proton and neutron compressible fluids moving within the rigid surface of the nucleus[38]. Danos improved the SJ model by including the GDR width, Γ_{GDR} [25, 39] in the second-sound hydrodynamic model[25, 39], where E_{GDR} and

Γ_{GDR} are related to $a_{\text{sym}}(A)$ as[30],

$$a_{\text{sym}}(A) = \frac{MA^2}{8\hbar^2 K^2 NZ} \frac{E_{\text{GDR}}^2}{1 - \left(\frac{\Gamma_{\text{GDR}}}{2E_{\text{GDR}}}\right)^2} \approx 1 \times 10^{-3} \left(\frac{A^{8/3}}{NZ}\right) \frac{E_{\text{GDR}}^2}{1 - \left(\frac{\Gamma_{\text{GDR}}}{2E_{\text{GDR}}}\right)^2}, \quad (9)$$

where K is the real eigenvalue of $\nabla^2 \rho_z + K^2 \rho_z = 0$, with the boundary condition $(\mathbf{n} \cdot \nabla \rho_z)_{\text{surface}} = 0$, and has a value of $KR = 2.082$ for a spherical nucleus[40]. For quadrupole deformed nuclei with an eccentricity of $a^2 - b^2 = \epsilon R^2$, where a and b are the half axes and ϵ the deformation parameter, the GDR lineshape splits into two peaks with similar values of Ka and $Kb \approx 2.08$ [39]. For deformed nuclei, we estimate a similar equation to Eq. 9, but using the average centroid energy and the FWHM of the total Lorentzian (see e.g.[41]). Uncertainties in the quoted values arise from the error propagation of Eq. 9.

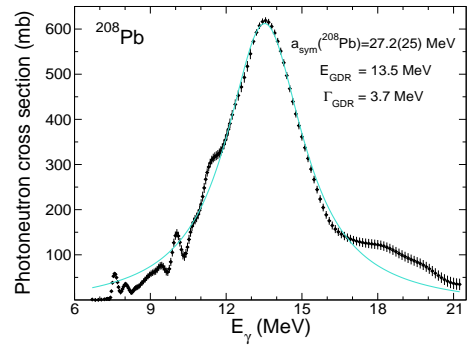


Figure 2: A Lorentzian fit to GDR data extracted for ^{208}Pb [32, 33].

The GDR cross-section data for each nucleus were obtained from the EXFOR and ENDF databases [32, 33] and fitted with one or two Lorentzian curves to extract E_{GDR} and Γ_{GDR} , as shown e.g. in Fig. 2 for ^{208}Pb . The data set for each nucleus was selected based on the number of data points, experimental method and energy range. In this work, the maximum integrated γ -ray energy, E_{γ}^{max} , was in the range 20–50 MeV, therefore excluding contributions resulting from high energy effects such as pion exchange and other meson resonances. The resulting distribution of $a_{\text{sym}}(A)$ is shown in the left panel of Fig. 3, which converges at approximately 27 MeV for heavy nuclei. It is reassuring that the two methods based on photoabsorption cross-section data –

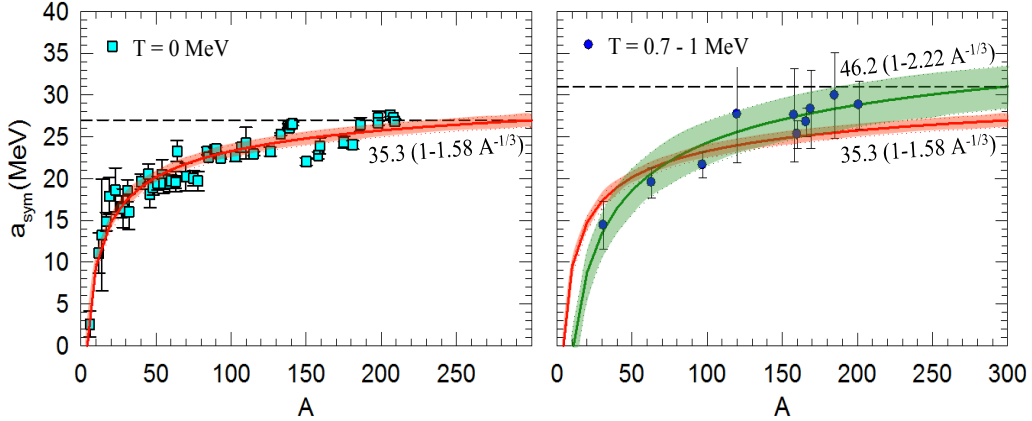


Figure 3: Symmetry energy coefficient, $a_{\text{sym}}(A)$, of finite nuclei as a function of mass number A extracted from GDRs built on ground states ($T = 0$) (left panel) and excited states ($T = 0.7 - 1$ MeV) (right panel) using Eq. 9.

namely $a_{\text{sym}}(A)$ extracted from σ_{-2} values and parameters of GDRs built on ground states – present similar trends.

Data obtained from GDR parameters at $T = 0$ can also be fitted to Eq. 2, which yields $a_{\text{sym}}(A) = 35.3(7)(1 - 1.58(5)A^{-1/3})$ MeV (red solid band in Fig. 3), with an RMS deviation of 15%. Larger values of $S_v = 42.8$ and $S_s = 89.9$ were determined by Berman using Eq. 9 for 29 nuclei ranging from $A = 75$ to 209 [42]. Furthermore, Berman argued that assuming a surface binding energy coefficient of $a_s = 20$ MeV in the SEMF, the large symmetry to surface energy ratio, $S_s/a_s = 4.5$, favors – as a result of a steeper slope of the binding energy curve for heavy nuclei – a close-in neutron dripline for heavy elements; hence, constraining the reaction network that produces heavy elements by the r-process in neutron mergers and supernovae. Using our value of $S_s = 46$ and $a_s = 20$ MeV, a more reasonable ratio of $S_s/a_s = 2.3$ is determined. Slightly smaller values of $a_s \approx 17$ MeV are also found in the literature [5, 36], yielding $S_s/a_s = 2.7$.

Furthermore, it is interesting to investigate the behavior of $a_{\text{sym}}(A)$ using the available information on GDRs built on excited states, below the critical temperatures and spins where the GDR width starts broadening; i.e. for moderate average temperatures of $T \lesssim T_c = 0.7 + 37.5/A$ MeV and spins J below the critical angular momentum $J \lesssim J_c = 0.6A^{5/6}$. In fact, similar centroid energies, $E_{\text{GDR}}^{\text{exc}}$, and resonance strengths, $S_{\text{GDR}}^{\text{exc}}$ – relative to the Thomas–Reiche–Kuhn E1 sum rule [27] – to those found for the ground-state counterparts [29, 43] indicate a common physical origin for all GDRs, in concordance with the Brink–Axel hypothesis that assumes that a GDR

can be built on every state in a nucleus [44, 45].

Applying again Eq. 9, the right panel of Fig. 3 shows $a_{\text{sym}}(A)$ values for GDRs built on excited states in slightly-deformed nuclei ^{31}P [46], ^{63}Cu [47], ^{97}Tc [48], ^{120}Sn [49] and ^{201}Tl [50], as well as for well-deformed nuclei in the $A \approx 160 - 180$ mass region ($^{158,160,166}\text{Er}$, ^{169}Tm and ^{185}Re [41, 51, 52]). With an average temperature between $T \approx 0.7$ and 1.0 MeV and below J_c , these nuclei were selected to investigate the symmetry energy at temperatures relevant to the r-process nucleosynthesis. Surprisingly, $a_{\text{sym}}(A)$ values for heavy nuclei are relatively larger than previously observed at $T = 0$ MeV. A fit to the data using Eq. 2 (green solid line in Fig. 3) yields $a_{\text{sym}}(A) = 46.2(2.4)(1 - 2.22(14)A^{-1/3})$ MeV, with an RMS deviation of 6%. A value of $a_{\text{sym}}(A) = 30$ MeV for heavy nuclei yields larger values of $S_v = 44.44$, $S_s = 97.32$ and $S_s/a_s = 4.87$ (again for $a_s = 20$ MeV). Two bands showing the loci limits of the two fitting curves at $T = 0$ and $T \approx 0.7 - 1$ MeV are shown for comparison. Such a distinct behaviour could clearly affect nucleosynthesis of heavy elements via the r-process during the cooling down of the ejecta.

Lighter or heavier seed nuclei are generally produced depending on the density and temperature of the ejecta gas. Assuming nuclear-statistical equilibrium – when forward and reverse reactions are balanced – abundances follow a Maxwell-Boltzmann distribution where lighter seed nuclei are favoured at very high temperatures ($\propto kT^{-3/2(A-1)}$) and heavier nuclei are favoured at very high densities ($\propto \rho^{A-1}$), as those found in the ejecta of neutron-star mergers [3]. At temperatures below $T = 1$ MeV (or 1.2×10^{10} K), seed nuclei are produced before charge reactions freeze out – impeded by

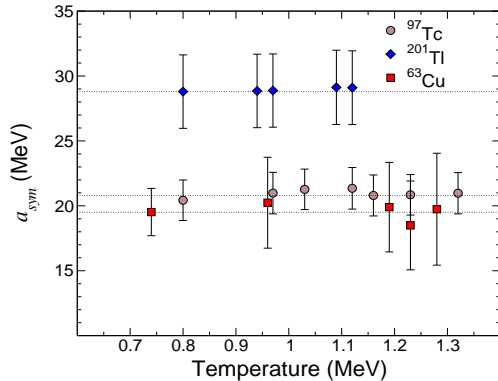


Figure 4: Symmetry energy coefficient, $a_{\text{sym}}(A)$ extracted for ^{63}Cu , ^{97}Tc and ^{201}Tl as a function of temperature, T . A similar constant behaviour is observed for other nuclei. The horizontal dotted lines are shown as a reference.

the Coulomb barrier – at about $T \approx 0.5$ MeV (or 5×10^9 K). Thereafter, heavy nuclei are produced through subsequent neutron capture until neutron reactions freeze out – as neutrons are finally consumed – at a few 10^8 K.

Our work may not be sensitive to the lower temperatures occurring during neutron capture in neutron-star mergers, which likely range from $T \approx 0.5 \times 10^8$ K [53] to $T \approx 5 \times 10^9$ K [54] (i.e. in the range from $T \approx 0.04$ to 0.43 MeV, respectively). Nevertheless, Fig. 4 shows that the symmetry energy does not change with temperature in the [0.74, 1.3] MeV range, which suggests that this relation may still hold at lower temperatures.

Such an increase in the symmetry energy results from the change in the effective mass of the nucleon, which decreases as T increases in the temperature interval $0 < T < 1$ MeV [55]. The temperature dependence of the symmetry energy has been studied within the liquid-drop and Fermi gas models [56], where an effective nucleon mass – the so-called ‘w’ mass – is introduced to account for the non-locality of the Hartree-Fock potential. This leads to an increase in the centroid energy of the GDR and, hence, the symmetry energy of medium and heavy mass nuclei also increases by approximately 8% at $T \approx 1$ MeV [55]. In the current work, we notice a slight increase of 3-5% in the centroid energy at $T \approx 0.7 - 1$ MeV as compared with the ground-state values for nearly-spherical ^{120}Sn [57], ^{208}Pb [58] and ^{201}Tl [50] nuclei as well as for the deformed nuclei in the $A = 160 - 180$ mass region [41, 51, 52]. Although such an increase is within the experimental errors, it leads to a distinct systematic behaviour, as shown in the right panel of Fig. 3.

Finally, the effects from the larger symmetry energy

at $T \approx 0.7 - 1$ MeV are illustrated in Fig. 5, which shows the corresponding nuclear charts (top) and binding energy curves (bottom) using $a_{\text{sym}} = 23.7$ MeV [60] (left) and 30 MeV (right), respectively. The nuclear chart determined using $a_{\text{sym}} = 30$ MeV illustrates a substantial close-in of the neutron dripline, as a result of the decreasing binding energy per nucleon in neutron-rich nuclei. For instance, the dripline closes in from ^{254}Pt to ^{220}Pt for $a_{\text{sym}} = 23.7$ and 30 MeV, respectively. Figure 6 shows the respective neutron driplines and clearly illustrates the dramatic effect of an enhanced symmetry energy in the production of heavy elements, which constrains exotic r-process paths and plausibly explains the universality of r-process abundances inferred from the observation of extremely metal-poor stars and our Sun.

Consequently, such an increase in the symmetry energy leads to the reduction of radiative neutron capture rates as neutron-rich nuclei become less bound. The corresponding change in the capture cross section has been calculated using TALYS [61] and EMPIRE [62] codes by changing only the mass excess with standard input parameters. Both codes yield similar results with a reduction of the neutron-capture cross section by a factor of the order of 10^2 in the $A \approx 200$ mass region relevant to the r-process. More detailed calculations will be presented in a separate manuscript. These findings support the rapid drop of the neutron capture rates at increasing neutron excesses inferred from Goriely’s microscopic calculations at $T = 1.5 \times 10^9$ K [12].

More experimental data regarding GDRs built on excited states below $T \approx 0.7$ MeV are crucially needed in order to elucidate the nature of the symmetry energy as a function of temperature. Modern high-efficient spectrometers such as GAMKA in South Africa [63] – with up to 30 HPGe clover and LaBr₃ detectors – may provide such data.

References

- [1] C. F. von Weizsäcker, Zur Theorie der Kernmassen. *Z. Phys.* **96** (1935) 431.
- [2] H. A. Bethe and R. F. Bacher, Stationary States of Nuclei, *Rev. Mod. Phys.* **8** (1936) 82.
- [3] F.-K. Thielemann, M. Eichler, I. V. Panov, and B. Wehmeyer, Neutron Star Mergers and Nucleosynthesis of Heavy Elements, *Annu. Rev. Nucl. Part. Sci.* **67** (2017) 253.
- [4] D. M. Siegel, J. Barnes, and B. D. Metzger, Collapsars as a major source of r-process elements, *Nature* **569** (2019) 241.
- [5] K. S. Krane, *Introductory Nuclear Physics*, Wiley (1987).
- [6] M. Kutschera, Nuclear symmetry energy and structure of dense matter in neutron stars, *Phys. Lett. B* **340** (1994) 1.
- [7] J. Piekarewicz, B. K. Agrawal, G. Colò, W. Nazarewicz, N. Paar, P.-G. Reinhard, X. Roca-Maza, and D. Vretenar, Electric dipole polarizability and the neutron skin, *Phys. Rev. C* **85** (2012) 041302(R).

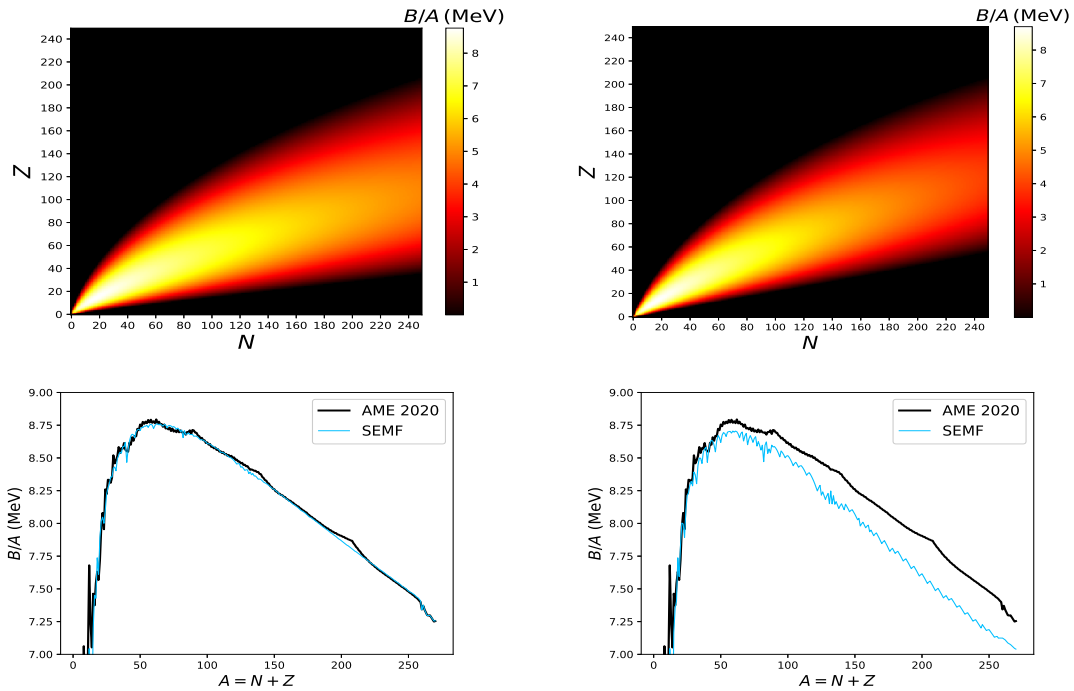


Figure 5: Nuclear charts (top panels) and binding energy curves (bottom panels) showing average binding energies per nucleon using the Bethe-Weizsäcker SEMF for $a_{\text{sym}} = 23.7$ [60] MeV (left) and $a_{\text{sym}} = 30$ MeV (right). Atomic masses in the bottom panels are extracted from the 2020 atomic mass evaluation (AME 2020) [59].

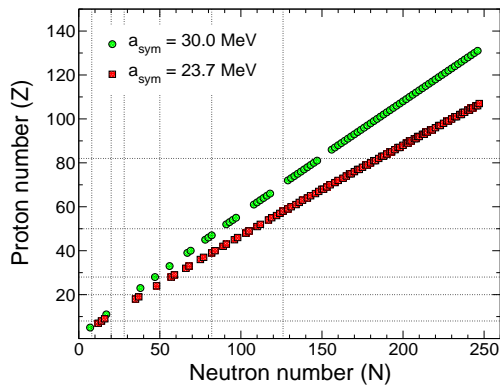


Figure 6: Neutron driplines predicted at symmetry energy coefficients of $a_{\text{sym}} = 23.7$ [60] (squares) and 30 MeV (circles). Dotted lines indicate the proton and neutron magic numbers.

- [8] K. Hebeler and A. Schwenk, Symmetry energy, neutron skin, and neutron star radius from chiral effective field theory interactions, *Eur. Phys. J. A* **50** (2014) 11.
- [9] A. W. Steiner, M. Prakash, J. M. Lattimer, and P. J. Ellis, Isospin asymmetry in nuclei and neutron stars, *Phys. Rep.* **411** (2005) 325.
- [10] J. M. Lattimer, Symmetry energy in nuclei and neutron stars, *Nucl. Phys. A* **928** (2014) 276.

- [11] J. M. Pearson, N. Chamel, A. F. Fantina, and S. Goriely, Symmetry energy: nuclear masses and neutron stars, *Eur. Phys. J. A* **50** (2014) 43.
- [12] S. Goriely, The r-process nucleosynthesis: a continued challenge for nuclear physics, *Nucl. Phys. A* **718** (2003) 287c.
- [13] J. J. Cowan, C. Sneden, J. E. Lawler, A. Aprahamian, M. Wiescher, K. Langanke, G. Martínez-Pinedo, and F. -K. Thielemann, Origin of the heaviest elements: The rapid neutron-capture process, *Rev. Mod. Phys.* **93** (2021) 015002.
- [14] B. D. Metzger, Kilonova, *Living Reviews in Relativity* **20** (2017) 3.
- [15] D. Watson *et al.*, Identification of strontium in the merger of two neutron stars, *Nature* **574** (2019) 497.
- [16] I. Bartos and S. Marka, A nearby neutron-star merger explains the actinide abundances in the early Solar System. *Nature* **569** (2019) 85.
- [17] N. Christlieb *et al.*, A stellar relic from the early Milky Way, *Nature* **419** (2002) 904.
- [18] C. Sneden, J. J. Cowan, and R. Gallino, Neutron-capture elements in the early galaxy, *Annu. Rev. Astron. Astrophys.* **46** (2008) 241.
- [19] Y.-Z. Qian, Supernovae versus neutron star mergers as the major r-process sources, *Astrophys. J.* **534** (2000) L67.
- [20] W. Aoki, S. Honda, T. C. Beers, T. Kajino, H. Ando, J. E. Norris, S. G. Ryan, H. Izumiura, K. Sadakane, and M. Takada-Hidai, Spectroscopic studies of very metal-poor stars with the Subaru high dispersion spectrograph. III. Light neutron-capture elements, *ApJ* **632** (2005) 611.
- [21] W. D. Myers and W. J. Swiatecki, Average nuclear properties, *Ann. Phys.* **55** (1969) 395.

- [22] J. Tian, H. Cui, K. Zheng, and N. Wang, Effect of Coulomb energy on the symmetry energy coefficients of finite nuclei, *Phys. Rev. C* **90** (2014) 024313.
- [23] J. M. Lattimer and Y. Lim, Constraining the symmetry parameters of the nuclear interaction, *ApJ* **771** (2013) 51.
- [24] L. Trippa, G. Colò, and E. Vigezzi, Giant dipole resonance as a quantitative constraint on the symmetry energy, *Phys. Rev. C* **77** (2008) 061304(R).
- [25] B. L. Berman and S. C. Fultz, Measurements of the giant dipole resonance with monoenergetic photons, *Rev. Mod. Phys.* **47** (1975) 713.
- [26] A. B. Migdal, Quadrupole and dipole gamma-radiation of nuclei, *J. Exptl. Theoret. Phys. U.S.S.R.* **15** (1945) 81.
- [27] J. S. Levinger, *Nuclear Photo-Disintegration*. Oxford University Press, Oxford (1960).
- [28] T. Kawano *et al.*, IAEA Photonuclear Data Library 2019, *Nucl. Data Sheets* **163** (2020) 109.
- [29] K. A. Snover, Giant Resonances in Excited Nuclei, *Ann. Rev. Nucl. Part. Sci.* **36** (1986) 545.
- [30] R. Bergere, Lecture Notes in Physics **61**, *Photonuclear Reactions I*, (Springer-Verlag, 1977).
- [31] J. N. Orce, Polarizability effects in atomic nuclei, *Int. J. Mod. Phys. E* **29** (2020) 2030002.
- [32] EXFOR: Experimental Nuclear Reaction Data. <https://www-nds.iaea.org/exfor/exfor.htm>
- [33] ENDF: Evaluated Nuclear Data File. <https://www-nds.iaea.org/exfor/endl.htm> (iaea.org)
- [34] J. N. Orce, New formulas for the (-2) moment of the photoabsorption cross section, σ_{-2} , *Phys. Rev. C* **91** (2015) 064602.
- [35] M. Wang, G. Audi, A. H. Wapstra, and F. G. Kondev, The AME2016 atomic mass evaluation (II), *Chin. Phys. C* **36** (2012) 1603.
- [36] P. Danielewicz, Surface symmetry energy, *Nucl. Phys. A* **727** (2003) 233.
- [37] H. Koura, T. Tachibana, M. Uno, and M. Yamada, Nuclidic mass formula on a spherical basis with an improved even-odd term, *Prog. Theor. Phys.* **113** (2005) 305.
- [38] H. Steinwedel, J. H. D. Jensen, and P. Jensen, Nuclear dipole vibrations, *Phys. Rev.* **79** (1950) 1019.
- [39] M. Danos, On the long-range correlation model of the photonuclear effect, *Nucl. Phys.* **5** (1958) 23.
- [40] Lord Rayleigh, *The Theory of Sound*, second edition (MacMillan Co., London, 1896) Chapter XVII.
- [41] J. J. Gaardhøje, A. M. Bruce, and B. Herskind, Nuclear collective motion under extreme conditions: the GDR at very high spin and temperature, *Nucl. Phys. A* **482** (1988) 121c.
- [42] B. L. Berman, Mass variation of the nuclear symmetry energy. *Proceedings of the International Conference on Photonuclear Reactions and Applications, Pacific Grove, California*, ed. by B. L. Berman (Lawrence Livermore Laboratory, Livermore) (1973) 569.
- [43] J. J. Gaardhøje, Nuclear structure at high excitation energy studied with giant resonances, *Annu. Rev. Nucl. Part. Sci.* **42** (1992) 483.
- [44] D. Brink, Some aspects of the interaction of light with matter. Doctoral thesis, Oxford University, 1955 (unpublished).
- [45] P. Axel, Electric dipole ground-state transition width strength function and 7-Mev photon interactions, *Phys. Rev.* **126** (1962) 671.
- [46] D. Mondal *et al.* Study of giant dipole resonance in hot rotating light mass nucleus ^{31}P , *Phys. Lett. B* **784** (2018) 423.
- [47] M. Kicińska-Habior, K. A. Snover, C. A. Gossett, J. A. Behr, G. Feldman, H. K. Glatzel, J. H. Gundlach, and E. F. Garman, Statistical giant dipole resonance decay of highly excited states of ^{63}Cu , *Phys. Rev. C* **36** (1987) 612.
- [48] B. Dey *et al.*, Probing the critical behavior in the evolution of GDR width at very low temperatures in $A \sim 100$ mass region, *Phys. Lett. B* **731** (2014) 92.
- [49] P. Heckman *et al.*, Low-temperature measurement of the giant dipole resonance width, *Phys. Lett. B* **555** (2003) 43.
- [50] D. Pandit, S. Mukhopadhyay, S. Pal, A. De, and S. R. Banerjee, Critical behavior in the variation of GDR width at low temperature, *Phys. Lett. B* **713** (2012) 434.
- [51] C. A. Gossett, K. A. Snover, J. A. Behr, G. Feldman, and J. L. Osborne, Deformation of heated nuclei observed in the statistical decay of the giant dipole resonance, *Phys. Rev. Lett.* **54** (1985) 1486.
- [52] D. Pandit *et al.*, Puzzle of collective enhancement in the nuclear level density, *Phys. Lett. B* **816** (2021) 136173.
- [53] S. Goriely, A. Bauswein, and H. -T. Janka, r-process nucleosynthesis in dynamically ejected matter of neutron star mergers, *ApJ Lett.* **732** (2011) L32.
- [54] Meng-Ru Wu, R. Fernández, G. Martínez-Pinedo, and B. D. Metzger, Production of the entire range of r-process nuclides by black hole accretion disc outflows from neutron star mergers, *MNRAS* **463** (2016) 2323.
- [55] P. Donati, P. M. Pizzochero, P. F. Bortignon, and R. A. Broglia, Temperature dependence of the nucleon effective mass and the physics of stellar collapse, *Phys. Rev. Lett.* **72** (1994) 2835.
- [56] P. F. Bortignon, A. Bracco, and R. A. Broglia, Giant Resonances: Nuclear structure at finite temperature, *Contemporary Concepts in Physics* (Routledge, 1998).
- [57] P. Heckman *et al.*, Low-temperature measurement of the giant dipole resonance width, *Phys. Lett. B* **555** (2003) 43.
- [58] T. Baumann *et al.*, Evolution of the giant dipole resonance in excited ^{120}Sn and ^{208}Pb nuclei populated by inelastic alpha scattering, *Nucl. Phys. A* **635** (1998) 428.
- [59] M. Wang, W. J. Huang, F. G. Kondev, G. Audi, and S. Naim, The AME 2020 atomic mass evaluation (II), *Chinese Phys. C* **45** (2021) 030003.
- [60] J. W. Rohlf, "Modern Physics from alpha to Z0", Wiley (1994).
- [61] A. J. Koning, S. Hilaire, and S. Goriely, (2015) *Talys User Manual*, <http://www.talys.eu/en/download-talys/>
- [62] M. Herman, *et al* (2007) EMPIRE: nuclear reaction model code system for data evaluation. *Nucl Data Sheets*. <https://doi.org/10.1016/j.nds.2007.11.003> 8:2655-2715
- [63] <https://www.nrf.ac.za/media-room/news/nrf-funds-state-art-nuclear-spectrometer-uwc>